Comparison of the Time-Reversal and SEABED Imaging Algorithms Applied on Ultra-Wideband Experimental SPR Data

A. Cresp [#1], M. J. Yedlin [†2], T. Sakamoto [*3], I. Aliferis [#4], T. Sato [*5], J.-Y. Dauvignac [#6], C. Pichot [#7]

[#]LEAT, Université de Nice-Sophia Antipolis, CNRS
250, rue Albert Einstein, 06560 Valbonne, France
[1]anthony.cresp@unice.fr
[4]iannis.aliferis@unice.fr
[6]jean-yves.dauvignac@unice.fr
[7]christian.pichot@unice.fr

[*]Department of Communications and Computer Engineering
Graduate School of Informatics, Kyoto University
Yoshida-Honmachi, Sakyo-ku, Kyoto 606-8501, Japan
[3]t-sakamoto@i.kyoto-u.ac.jp
[5]tsato@kuee.kyoto-u.ac.jp

[†]Department of Electrical and Computer Engineering, University of British Columbia
2332 Main Mall, Vancouver, B.C., Canada V6T 1Z4
[2]matty@ece.ubc.ca

Abstract—**This paper presents a comparison study between a simple time-reversal algorithm (designed at LEAT) and the SEABED algorithm (designed at Kyoto University) with their application to multiple-target experiments. Data are collected with an eight element ultra-wideband antenna linear array connected to an eight port vector network analyzer, working in a frequency bandwidth starting from 1.5 GHz up to 8 GHz. Several target configurations demonstrate the advantages and disadvantages of both algorithms.**

I. Introduction

In Surface-Penetrating Radar (SPR) applications, such as security or landmine detection for instance, signal processing plays a key role in obtaining images of targets. Different algorithms have been developed for that purpose, combining preprocessing methods and microwave imaging [1]. Among these, two algorithms, time-reversal [2] and the Shape Estimation Algorithm based on BST and Extraction of Directly scattered waves (SEABED) [3], are promising algorithms for the detection of the location of multiple scatterers. The efficiency of time-reversal has already been shown in the case of embedded targets [4], [5] and also in telecommunication applications, taking advantages of the multipath environment [6], [7], while SEABED has been seen as a promising candidate due to its high-speed processing property.

Here we compare time-reversal and correlation (in effect an adjoint method) and the SEABED algorithms applied on experimental data, obtained in a multiple-target SPR measurement configuration. The measurement configurations (radar and geometric configuration of radar scenes) are presented in Section II while the algorithms are presented in Section III

and IV. In section V we discuss the results and advantages of each method. Section VI contains a final discussion and conclusion.

II. Measurement Setup

A. Measurement system

The antennas used to build the array are ETS (Exponentially Tapered Slot) antennas based on Vivaldi type antennas [8]. These antennas have been employed in array experiment by Chatelée [9] and have a flat S_{11} response from 1.4 to 20 GHz. For the experiments we present hereafter, the antenna array is an 8-element linear array with a spacing of 8 cm between each antenna. It is connected to an 8-port Rohde & Schwarz ZVT multi-port vector network analyzer which is employed over the frequency range from 1.5 to 8 GHz with 2001 frequency points. In this configuration we can have access up to 64 measured S parameters in a short time.

B. Configuration of radar scenes

Several data acquisitions were used in order to obtain the results presented in section V. Targets were dielectric or metal scatterers, placed on a grid for easier location, as we can see in Fig. 1. Measurements were made in free space and we assume a two-dimensional reconstruction for simplicity. For all the experiments, multiple-target configurations were studied.

For the two-target case, we use a metallic cylinder with a radius of 2.5 cm and a plastic bottle with a radius of 4 cm filled with saline to approximate human's body permittivity. The second configuration corresponds to four aligned plastic bottles filled with water except for the second one from the

left which is the saline bottle. They were placed 60 cm from the front of the antenna array and were spaced 20 cm apart. For the last configuration, we used the same bottles placed in a diagonal direction on the grid, the first one being the bottle of saline.

Fig. 1. Illustration of measurement configuration. The antenna array can be seen in the top right corner of the image while targets are positioned on a grid placed in front of the array.

III. TIME-REVERSAL IMAGING ALGORITHM

The algorithm we use herein is an adaptation of time-reversal imaging [10] and adjoint methods used in seismology [11]. We use Claerbout's definition of a reflector [12] – the time coincidence of the downgoing wavefield from the source and the reflected wavefield. The assumption here is that the source wavefield represents the downgoing or incident wavefield and that the receiver wavefield consists of the upgoing wavefield. The time-coincidence of the two wavefields can be computed by obtaining the zero-lag cross-correlation between these wavefields at any candidate reflecting point, allowing us to get a single image of the target locations, even if energy is not focusing at the same time at the scatterer positions as in classical time-reversal processing, applied to single targets.

In practice the algorithm consists of the following steps:
1) Propagate the downgoing wavefield from the transmitting antenna to the candidate reflecting point to obtain $d(t)$;
2) Time-reverse the recorded wave field at the receiver and back-propagate it to the same candidate reflecting point to obtain $u(t)$;
3) At the candidate reflecting point compute the zero-lag cross-correlation between $d(t)$ and the time reverse of $u(t)$.

In order to use the foregoing algorithm on real data, a representative wavelet must be extracted and the antenna spatial source characteristics must be estimated. We extract a representative wavelet directly from the data and use a dipole approximation for the source, which we project onto a plane. The final two-dimensional image obtained is a stack over all data collected by the antenna array. In this data acquisition

each antenna acts as a transmitter and all antennas receive the reflected wavefields from the targets.

IV. THE SEABED IMAGING ALGORITHM

The SEABED algorithm, based on a reversible transform between the target shape and the received data, and suited to imaging with the UWB radar, can be used to estimate the target shape. The foregoing transform is a rigorous mathematical solution of the inverse scattering problem.

The SEABED algorithm is based on the application of a matched filter to the signals to pick the maximum peaks in the data. This matched filter is constructed as the Fourier transform of the reference signal measured previously. The curved line (X_T, X_R, Y), called a quasi-wavefront, is estimated by connecting the picked points. For multiple targets, we extract the other quasi-wavefronts as follows [13]. We subtract the reference signal from the received signals by changing the delay time and the amplitude as estimated when extracting the first quasi-wavefront. We apply the same method to the residual signals to obtain other quasi-wavefronts.

After these procedures, we apply the IBBST (Inverse Bistatic Boundary Scattering Transform) [14] expressed as:

$$x = X - \frac{2Y^3 Y_X}{Y^2 - d^2 + \sqrt{(Y^2 - d^2)^2 + 4d^2 Y^2 Y_X^2}}$$
$$y = \frac{\sqrt{Y^2 - d^2}}{Y}\sqrt{Y^2 - (x - X)^2}$$

where $X = \frac{X_T + X_R}{2}$ and $d = \frac{X_T - X_R}{2}$ are assumed and $Y_X = \frac{dY}{dX}$. This transform allows one to obtain the image without any iteration or repetition process only if the quasi-wavefront is accurately estimated.

V. IMAGING RESULTS

Figures 2, 4 and 6 show the results of the adjoint time-reversal processing while figures 3, 5 and 7 illustrate the application of the SEABED algorithm on the same dataset. For these experiments, we assume that there weren't any targets located at less than 15 cm from the front of the array. Considering this assumption, the beginning of each signal (up to 1 ns) can be time-gated in order to remove artifacts like residuals of the direct coupling between the antennas.

For the three measurement configurations, we note that targets are well-resolved and retrieved at the correct locations using the adjoint time-reversal processing. Nevertheless some artifacts are clearly seen and decrease the image quality. These are mainly due to the fact that the reconstruction was made on the differential dataset with very simple pre-processing. An example of raw data is presented in Fig. 8 where we can see direct coupling between antennas and environmental effects that weren't removed completely by the differential measurement. Direct coupling can be removed by time gating as explain above but we will still suffer from residual environmental artifacts. Due to the large amount of data, adjoint time-reversal processing was applied only to the investigation area that included all the targets. In order to keep the same
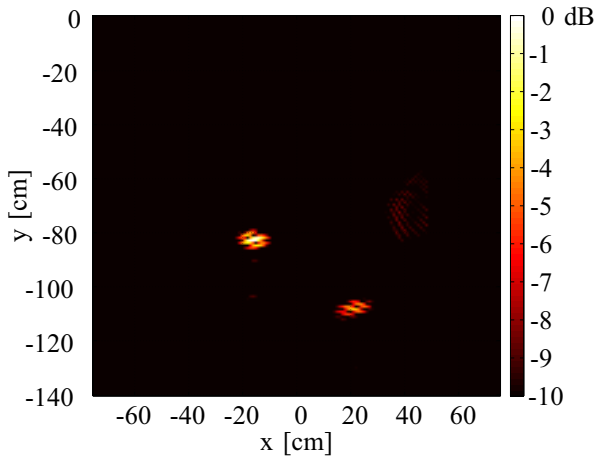
Fig. 2. Adjoint time-reversal result for a two-target configuration. The metal target was located at 80 cm from the front of the array and dielectric target at approximately 110 cm.
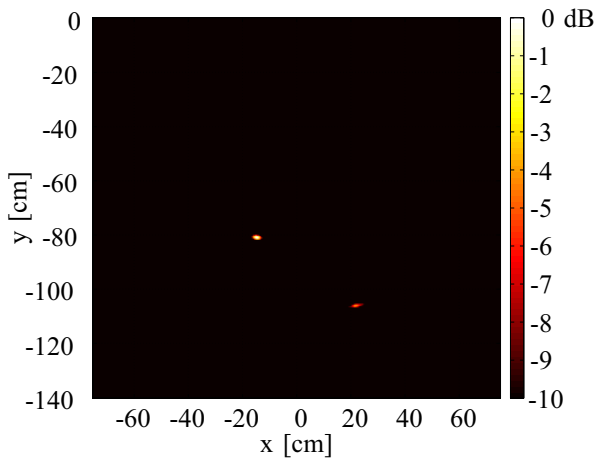

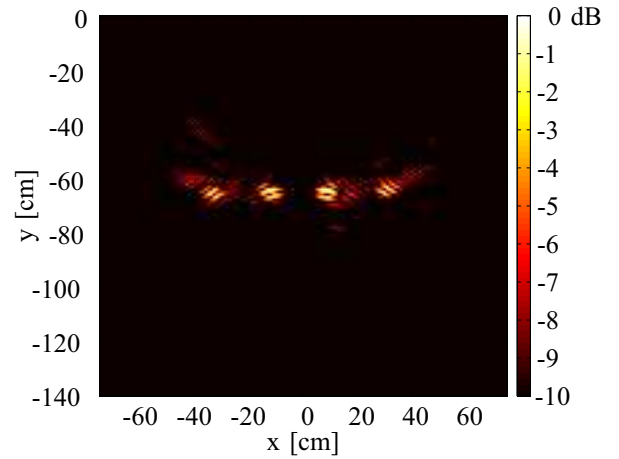Fig. 3. SEABED result for the same configuration as fig 2.

Fig. 4. Adjoint time-reversal result for a inline four dielectric target configuration. The dielectric targets were located at 60 cm from the front of the array.
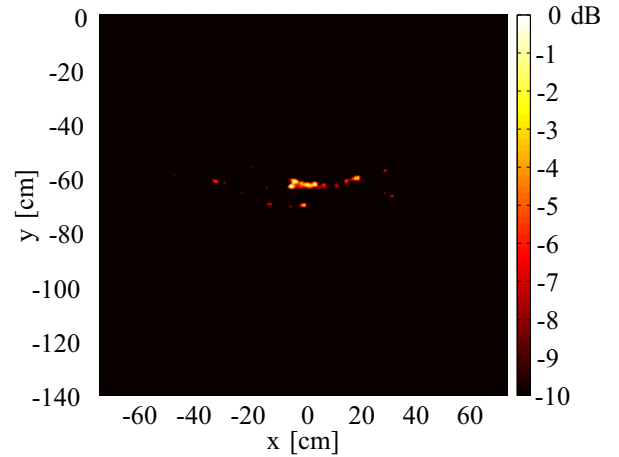

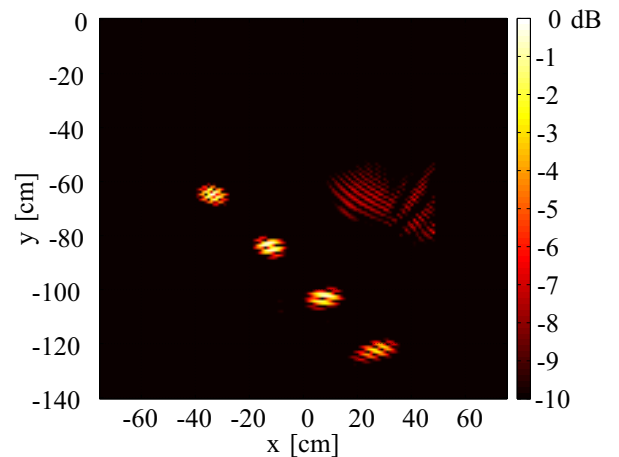Fig. 5. SEABED result for the same configuration as fig 4.

Fig. 6. Adjoint time-reversal result for a diagonal four dielectric target configuration. The first dielectric target was located at 60 cm from the front of the array.
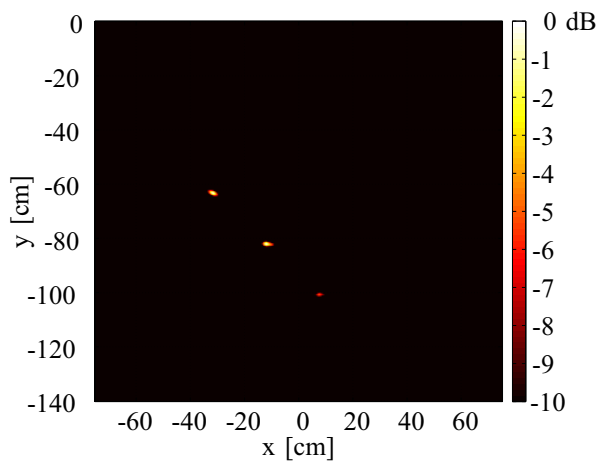
aspect ratio as the SEABED results, zero padding was done on the image borders.

If we compare the time-reversal results with the SEABED processing results, we see that, for the two-target case shown in Fig. 3, the resolution is significantly enhanced. Focusing occurs on the front interface of the targets which leads to efficient detection. However, if we look at the two four-target cases, in Fig. 5, the SEABED algorithm does not work properly, mainly due to the fact that this particular target configuration gives recorded signals with scatterer echoes very close to each other. This proximity leads to interference which affect the quasi-wavefront extraction procedure as we can see by comparing Fig. 9 and Fig. 10. The diagonal four-target case presented in the Fig. 7 works well despite the fact that the furthest target is not detected. The other three targets are detected at the proper locations and we obtain very good resolution.

VI. CONCLUSIONS

In this paper, we presented inverse scattering imaging results, using the SEABED method and the combination of

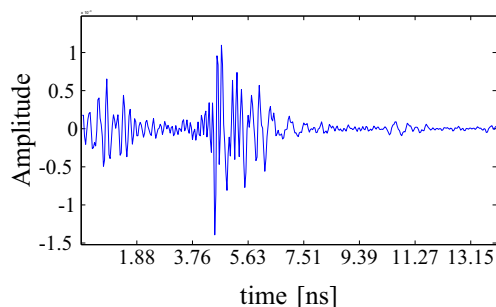Fig. 7. SEABED result for the same configuration as fig 6.

Fig. 8. An exemple of one of the measured signals coming from the scatterers for the four diagonal target case.
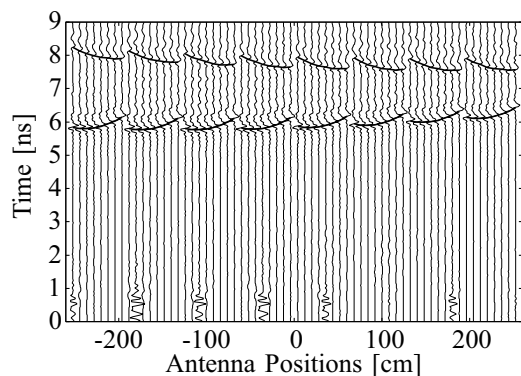

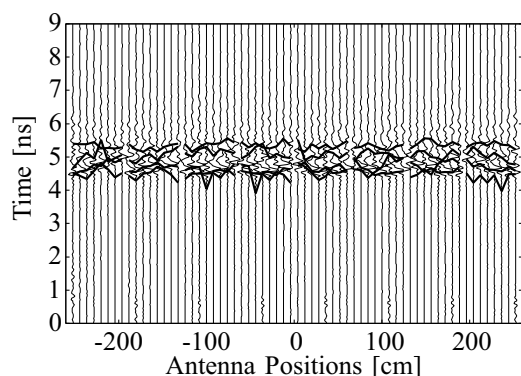Fig. 9. Extracted quasi-wavefronts from the two-target case measured signals.

Fig. 10. Extracted quasi-wavefronts from the inline four-target case measured signals.

conventional time-reversal processing with adjoint methods, on measured data obtained using an eight element UWB linear antenna array.

This study showed that the SEABED method gives, under certain conditions, high-resolution images leading to very good results, but does not work for all the measurements, especially when the targets are close together. A reliable method for quasi-wavefront extraction, making the SEABED algorithm more efficient regardless of target configuration, is under investigation.

On the other hand, adjoint time-reversal processing gives stable results for all the configurations, with all targets detected at the correct position. Proper pre-processing of the collected data and a better estimation of the wavelet shape, used in the adjoint reconstruction will improve the image quality. These improvements are currently being implemented.

REFERENCES

[1] D. J. Daniels, *Ground Penetrating Radar*, 2nd ed., ser. IEE Radar, Sonar, Navigation and Avionics Series. London: The Institution of Electrical Engineers, 2004, no. 15.
[2] M. Fink, D. Cassereau, A. Derode, C. Prada, P. Roux, M. Tanter, J.-L. Thomas, and F. Wu, "Time-reversed acoustics," *Reports on Progress in Physics*, vol. 63, no. 12, pp. 1933–1995, December 2000.
[3] T. Sakamoto, "A fast algorithm for 3-dimensional imaging with UWB pulse radar systems," *IEICE Trans. on Commun.*, vol. E90-B, no. 3, pp. 636–644, March 2007.
[4] G. Micolau and M. Saillard, "D.O.R.T. method as applied to electromagnetic subsurface sensing," *Radio Science*, vol. 38, no. 3, pp. 4_1–4_12, May 2003.
[5] G. Micolau, M. Saillard, and P. Borderies, "DORT Method as Applied to Ultrawideband Signals for Detection of Buried Objects," *IEEE Transactions on Geoscience and Remote Sensing*, vol. 41, no. 8, pp. 1813–1819, August 2003.
[6] G. Lerosey, J. de Rosny, A. Tourin, A. Derode, G. Montaldo, and M. Fink, "Time reversal of electromagnetic waves and telecommunication," *Radio Science*, vol. 40, no. 5, p. RS6S12, September 2005.
[7] A. E. Akogun, R. C. Qiu, and N. Guo, "Demonstrating Time Reversal in Ultra-wideband Communications Using Time Domain Measurements," Knoxville, Tennessee, May 8–11, 2005.
[8] E. Guillanton, J.-Y. Dauvignac, C. Pichot, and J. Cashman, "A new design tapered slot antenna for ultra-wideband applications," *Microwave and Optical Technology Letters*, vol. 19, no. 4, pp. 286–289, November 1998.
[9] V. Chatelée, "Développement d'un système d'imagerie microonde multistatique ultra large bande. Application à la détection d'objets en régime temporel et fréquentiel," Ph.D. dissertation, Université de Nice – Sophia Antipolis, December 2006.
[10] M. Fink, "Time-reversal mirrors," *Journal of Physics D: Applied Physics*, vol. 26, no. 9, pp. 1333–1350, September 1993.
[11] A. Tarantola, "Inversion of seismic reflection data in the acoustic approximation," *Geophysics*, vol. 49, no. 8, pp. 1259–1266, August 1984.
[12] J. F. Claerbout, "Toward a unified theory of reflector mapping," *Geophysics*, vol. 36, no. 3, pp. 467–481, 1971.
[13] S. Hantscher, A. Reisenzahn, and C. G. Diskus, "Throught-wall imaging with a 3-D UWB SAR algorithm," *IEEE Signal Processing Letters*, vol. 15, pp. 269–272, 2008.
[14] S. Kidera, Y. Kani, T. Sakamoto, and T. Sato, "A fast and high-resolution 3-D imaging algorithm with linear array antennas for UWB pulse radars," *IEICE Trans. on Commun.*, vol. E91-B, no. 8, pp. 2683–2691, 2008.